



Scaling-Relation Kinetic Monte Carlo Simulations for CO Oxidation over Dilute Pt@Au Alloys

Downloaded from: <https://research.chalmers.se>, 2025-12-10 01:14 UTC

Citation for the original published paper (version of record):

Bosio, N., Grönbeck, H. (2024). Scaling-Relation Kinetic Monte Carlo Simulations for CO Oxidation over Dilute Pt@Au Alloys. *Journal of Physical Chemistry C*, 128(21): 8621-8627.
<http://dx.doi.org/10.1021/acs.jpcc.4c01263>

N.B. When citing this work, cite the original published paper.

Scaling-Relation Kinetic Monte Carlo Simulations for CO Oxidation over Dilute Pt@Au Alloys

Published as part of *The Journal of Physical Chemistry C* virtual special issue "Jens K. Nørskov Festschrift".

Noemi Bosio and Henrik Grönbeck*



Cite This: *J. Phys. Chem. C* 2024, 128, 8621–8627



Read Online

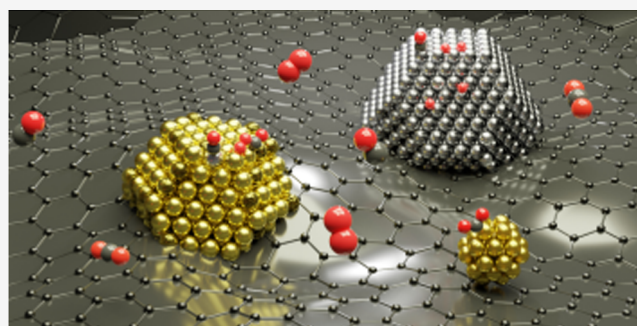
ACCESS |

Metrics & More

Article Recommendations

Supporting Information

ABSTRACT: Catalytic low-temperature CO oxidation continues to be an important materials challenge. Technological catalysts are commonly based on Pd and Pt nanoparticles, which are CO poisoned at low temperatures, hindering O₂ adsorption. Using first-principles-based kinetic Monte Carlo simulations, we explore dilute Pt@Au nanoalloys as a possibility to enhance the low-temperature activity by spatially separating CO and O₂ adsorption. CO is on these systems absorbed on Pt sites, whereas O₂ reacts molecularly from Au sites to form OCOO, which decomposes to CO₂ and O. The dilute Pt@Au systems are found to have a higher activity than pure Au systems in a temperature range not accessible to Pt-only catalysts. The results show that dilute Pt@Au alloys in combination with Pt-only catalysts have the potential for CO oxidation in a wide temperature range.



INTRODUCTION

CO oxidation is a widely studied catalytic reaction motivated by the need to control emissions from the incomplete combustion of hydrocarbons. The main challenge is to achieve sufficient activity at low temperatures, which within automotive applications is termed the cold-start problem. In fact, about 80–90% of all automotive CO emissions are emitted during the first minute of operation when the catalyst has not been heated enough by the exhaust gas.^{1,2} Thus, it is critical to develop catalytic materials with enhanced low-temperature activity to enable the emission control of cold exhaust streams.

The technological catalyst for CO oxidation is commonly based on precious metal Pd and/or Pt nanoparticles (NPs) supported on porous oxides. However, self-poisoning of CO prevents low-temperature oxidation as temperatures above 150 °C typically are required to obtain an appreciable activity.³ The self-poisoning originates from the high CO desorption energy combined with the fact that dissociative O₂ adsorption requires two metal sites. Thus, the catalyst temperature needs to be high enough to reduce the CO coverage and thereby increase the probability of having two vacant nearest neighbor sites.

Different strategies have been explored to enhance the low-temperature activity of CO oxidation.⁴ One materials strategy is to support the metal on a reducible oxide serving as an oxygen buffer and thereby providing an additional path for the reaction.⁵ CO adsorbed on the perimeter of a metal nanoparticle supported on a reducible oxide can react with lattice oxygen from the oxide through a Mars van Krevelen

mechanism.^{6,7} The formed oxygen vacancies are replenished by direct O₂ adsorption on the oxide. Thus, this mechanism does not require two empty metal sites for O₂ adsorption. The CO adsorption energy on typical reducible oxides such as TiO₂ and CeO₂ is low, which leads to efficient site separation for O₂ and CO adsorption. The activity for CO oxidation over Pt supported on CeO₂ is in this way limited by the activation energy of the CO + O reaction at the Pt/CeO₂ perimeter rather than the CO desorption energy.⁵ The coverage of CO on the metal phase becomes, at high enough temperatures, low enough for the reaction to proceed according to the conventional Langmuir–Hinshelwood mechanism.⁵

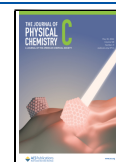
Another materials strategy to achieve low-temperature oxidation is to reduce the relative bond strength of CO with respect to O₂. One example is Au-based catalysts, which have been measured to be active for CO oxidation at temperatures as low as –80 °C.^{8,9} The catalytic activity of Au-based catalysts has a strong particle size dependence, with a high activity for particles with a diameter below 5 nm.⁸ The activity is related to the presence of under-coordinated sites where O₂ adsorbs with a high enough adsorption energy.¹⁰ CO oxidation on Au NPs

Received: February 27, 2024

Revised: April 25, 2024

Accepted: April 30, 2024

Published: May 20, 2024



has been suggested to occur via the formation of an OCOO intermediate, which decomposes to CO₂ and O.¹¹ The oxygen atom resulting from the OCOO decomposition can further react with CO to form a second CO₂ molecule. The Au-based catalysts are not sensitive to CO self-poisoning, despite the fact that the CO adsorption energy could be higher than that of O₂ as O₂ in this case requires only one adsorption site. One challenge with Au-based catalysts is the low activity at high temperatures due to the weak adsorption energies, which results in low coverages.

One potential possibility to enhance the low-temperature activity of both Pd/Pt and Au catalysts is alloying. Bimetallic alloys of Au–Ag,¹² Au–Ir,¹³ and Au–Pt¹⁴ have been measured to have higher CO oxidation activity than pure Au catalysts. Recently, dilute alloys have been explored for a range of different hydrogenation reactions.^{15–19} Dilute Au alloys are Au systems doped with a small number of transition metal monomers. Dilute alloys offer the possibility of spatially separating the different parts of the reactions. One example is partial acetylene hydrogenation over Pd@Cu, where H₂ dissociates over the Pd sites, whereas acetylene adsorbs on the Cu sites.¹⁸

In this study, we use density functional theory (DFT) calculations in combination with scaling-relation kinetic Monte Carlo (kMC) simulations to investigate low-temperature CO oxidation over dilute alloying of Au with Pt. The results are compared with the activities of pure Au systems and a Pt nanoparticle. We note that previous kinetic studies on CO oxidation over Au-systems^{11,20,21} mainly have been performed with mean-field models. kMC simulations have previously been performed for small clusters, which are governed by quantum size effects.²² Here, we address CO oxidation over Au and Pt@Au with an explicit treatment of the inhomogeneity of NPs having a range of different types of sites.

COMPUTATIONAL METHOD

DFT calculations are performed using the Vienna Ab-initio Simulation Package (VASP).^{23–25} The interactions between the valence electrons and the cores are described with the plane augmented wave method.^{26,27} Electrons treated in the valence are 2s²2p² (C), 2s²2p⁴ (O), 5d⁹6s¹ (Pt), and 5d¹⁰6s¹ (Au). The exchange–correlation effects are described using the generalized gradient approximation according to Perdew, Burke, and Ernzerhof.²⁸ van der Waals interactions are accounted for by including the correction proposed by Grimme et al. (D3).²⁹ The Kohn–Sham orbitals are expanded with plane waves using a 450 eV energy cutoff. Structures are optimized with the conjugate gradient method, and geometries are considered to be converged when the largest force is smaller than 0.02 eV/Å. The integration over the Brillouin zone is approximated by finite sampling using a Monkhorst–Pack scheme.^{30,31} The slabs are in all cases separated by at least 10 Å of vacuum. The energies in the kinetic models are zero-point-corrected using vibrational modes calculated within the harmonic approximation using finite differences.

The time evolution is in kMC simulations, described by events that connect different states of the system. The time is here evolved using the first reaction method,³² as implemented in ref 33. Considering two states (α and β) of the system, the time at which an event changes the system from α to β ($t_{\beta\alpha}$) is given by

$$t_{\beta\alpha} = t - \frac{1}{W_{\beta\alpha}} \ln(r) \quad (1)$$

where t is the current simulation time, $W_{\beta\alpha}$ is the reaction rate, and r is a uniform random number on the unit interval. The possible events are stored in a list of events, and the first event in the list is executed. The list of events and reaction rates is updated after each executed event by removing disabled events and adding enabled events. The update is done locally, as only events close to the executed event are affected.

The rate constants for adsorption are calculated using the collision theory

$$W_{ij}^{\text{ads}} = \frac{S_{i,j}^0 p_i A_{\text{site}}}{\sqrt{2\pi M_i k_B T}} \quad (2)$$

Here, i is the type of reactant (CO or O₂), j is the site index, $S_{i,j}^0$ is the sticking coefficient, p_i is the pressure of reactant i , A_{site} is the area of the site, M_i is the mass of the adsorbing molecule, k_B is the Boltzmann constant, and T is the temperature. The sticking coefficient for CO and O₂ adsorption is generally low for noble-metal surfaces.³⁴ As the O₂ and CO sticking coefficients for the present systems are unknown, we have set all sticking coefficients to 0.1. As CO adsorption/desorption are in equilibrium and O₂ adsorption is treated via the equilibrium constant (see below), the results are not sensitive to the choice of the sticking coefficient.³⁵ The desorption rate constants are obtained by the equilibrium constant ($K_{i,j}$) for adsorption and desorption

$$W_{ij}^{\text{des}} = \frac{W_{ij}^{\text{ads}}}{K_{i,j}} \quad (3)$$

The equilibrium constant is approximated by

$$K_{i,j} = \exp \left[\frac{-E_{i,j}^{\text{ads}} + T(S_i^{\text{ads}} - S_i^{\text{gas}})}{k_B T} \right] \quad (4)$$

where $E_{i,j}^{\text{ads}}$ is the adsorption energy of reactant i on site j . S_i^{gas} and S_i^{ads} are the entropies of the species in gas phase and adsorbed phase, respectively. The entropies of the adsorbed species are calculated in the harmonic approximation.³⁶

Transition state theory³⁷ is used to calculate the rate constant for the oxidation reaction

$$W_j = \frac{k_B T}{h} \left(\frac{Z^{\text{TS}}}{Z^{\text{IS}}} \right) \exp \left(\frac{-E_j}{k_B T} \right) \quad (5)$$

Here, Z^{TS} and Z^{IS} are the partition functions for the transition and initial states, respectively, and E_j is the reaction barrier. The partition function of the transition state (Z^{TS}) does not include the reaction coordinate, which yields the factor $\frac{k_B T}{h}$.

One challenge in kMC simulations is the separation in timescales for different events. For the considered systems, the O₂ adsorption and desorption events are fast with respect to the other events. To account for this problem, the probability (coverage) of having O₂ adsorbed on a site j is given by the equilibrium constant ($K_{\text{O}_2,j}$) for the considered site.³²

$$\theta_{\text{O}_2} = \begin{cases} 0, & \text{if the site is occupied by CO} \\ \frac{K_{\text{O}_2,j}}{1 + K_{\text{O}_2,j}}, & \text{if the site is unoccupied} \end{cases} \quad (6)$$

CO oxidation is studied as a function of temperature for a range of model systems with a total pressure of 40 Torr and a $p_{\text{O}_2}/p_{\text{CO}}$ ratio of 5. The presented results are averages of 10 different simulations, from which the standard deviations are evaluated. The turnover frequency (TOF) is calculated as the number of formed CO_2 molecules per surface atom in the system. We note that the calculated TOFs are sensitive to the calculated adsorption energies and reaction barriers, which make trends between different systems more relevant than the absolute TOFs and ignition temperatures.

MODEL SYSTEMS

The reaction kinetics is investigated over Au(111), Au(211), Au_{38} , and NPs of sizes 2 nm (309 atoms) and 3.2 nm (976 atoms) in the shape of truncated octahedra. The systems are studied either as pure Au-systems or with Pt monomers embedded in the surface of the Au-hosts. The dilute alloys with Pt embedded in Au(111) and Au(211) are denoted as Pt@Au(111) and Pt@Au(211), respectively. Pt monomers are in the NPs placed either in the (111) facet [Pt@NP(111)] or in an edge between two (111) facets [Pt@NP(edge)]. The systems with Pt embedded in the Au hosts are shown in Figure 1.

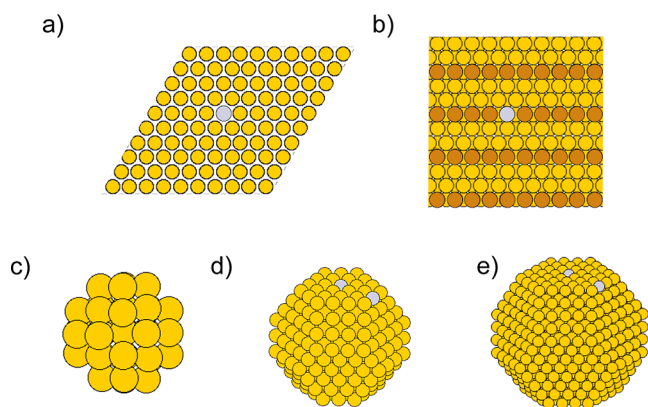
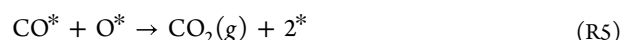
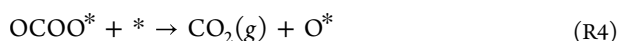
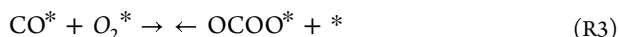
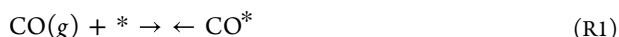


Figure 1. (a) Pt@Au(111), (b) Pt@Au(211), (c) Au_{38} , (d) Pt@NP (2 nm), and (e) Pt@NP (3.2 nm). For simplicity, Pt@NP(111) and Pt@NP(edge) are here combined in one Au NP structure. Atomic color code: Au (yellow) and Pt (gray). Step sites on Au(211) are colored brown.

The considered elementary steps (events) are adsorption and desorption of CO and O_2 , adsorbate diffusion, and the formation of CO_2 from either decomposition of the OCOO intermediate or reaction between adsorbed CO and O. We assume immediate desorption of CO_2 . The reaction steps are



where (g) represents gas-phase molecules and * denotes a surface site.

The energy landscapes for the reactions are calculated for Au(111), Au(211), and a Pt monomer embedded in Au(111) and Au(211), as shown in Table 1. The Pt monomer is

Table 1. Calculated Adsorption Energies (eV) without Zero-Point Corrections for CO, O_2 , and O over Au(111) and Au(211) as well as Pt Embedded in Au(111) and Au(211)^a

	$E_{\text{CO}}^{\text{ads}}$	$E_{\text{O}_2}^{\text{ads}}$	$E_{\text{O}}^{\text{ads}}$
Au(111)	−0.38	0.00	−0.07
Au(211)	−0.74	−0.31	−0.20
Pt@Au(111)	−1.65	−0.38	−0.33
Pt@Au(211)	−1.99	−0.76	−0.78
Au–Pt@Au(111)	−0.35	0.03	0.08
Au–Pt@Au(211)	−0.72	−0.20	−0.21

^aFor Pt@Au(111) and Pt@Au(211), the adsorption energies correspond to adsorption on the embedded Pt, whereas Au–Pt@Au(111) and Au–Pt@Au(211) correspond to adsorption on the Au site close to the embedded Pt.

preferentially embedded in Au(111) by 0.24 eV. The adsorption energies on Au(111) are weak, and the O_2 adsorption energy is zero. Adsorption on the undercoordinated Au(211) sites increases the adsorption energies. The adsorption energies are clearly higher on embedded Pt monomers where the values are close to the corresponding cases for pure Pt.⁵ To retrieve the experimentally measured atop adsorption site for CO on Pt with DFT, the CO adsorption energy on Pt is corrected by ΔE_{corr} (in eV) based on the C–O stretch vibration (ν_{CO} in cm^{-1}) according to ref 38.

$$\Delta E_{\text{corr}} = 1.8 - 0.0008 \cdot \nu_{\text{CO}} \quad (7)$$

Au sites close to the embedded Pt site have adsorption properties similar to those of the pure Au systems. Thus, Pt does not markedly alter the chemical properties of the neighboring Au sites.

To describe the energy landscape over the NPs, we use scaling relations^{39,40} with respect to the generalized coordination number (GCN) for CO, O_2 , and O adsorption. The GCN for a site i is given by⁴¹

$$\text{GCN}(i) = \sum_j \frac{\text{CN}(j)}{\text{CN}_{\text{max}}} \quad (8)$$

The sum runs over all nearest neighbors to site i . CN_{max} is 12 for both gold and platinum, which are fcc crystals. The GCN accounts for the second coordination shell, making it possible to distinguish different sites in the particle. Each atom in the surface layer is represented by a coarse-grained site. A single coarse-grained site contains the possible geometrical adsorption sites (atop, bridge, fcc, and hcp), and the energies used in the scaling relations refer to the preferred geometrical adsorption site. The connectivity between sites is accounted for by a nearest neighbor list.

The scaling relations between adsorption energies and GCN are obtained by calculating the adsorption energies for a set of model systems. The considered model systems are treated with (3×3) surface cells using four atomic layers and a $(7 \times 7 \times 1)$ Monkhorst–Pack sampling. The bottom two layers are fixed to

the corresponding bulk positions. CO adsorption is considered on Au(111), Au(100), Au(211), and two Au adatoms on Au(100) where CO is adsorbed in an atop site. The obtained scaling relation (see Supporting Information) is (in eV)

$$E_{\text{CO}}^{\text{ads}} = 0.118 \cdot \text{GCN} - 1.4126 \quad (9)$$

The scaling relations (in eV) for O₂ and O were adopted from our recent work using the same computational approach¹⁹

$$E_{\text{O}_2}^{\text{ads}} = 0.176 \cdot \text{GCN} - 1.247 \quad (10)$$

$$E_{\text{O}}^{\text{ads}} = 0.058 \cdot \text{GCN} - 0.566 \quad (11)$$

The scaling relations are reported here without zero-point corrections, which, however, are added in the kinetic simulations.

Having the adsorption energies from the present work, the activation barriers of reactions R3, R4, and R5 are obtained using the slopes of the scaling relations for three-dimensional clusters in ref 21. The adsorption energies and barriers define the potential energy surfaces for the reaction. The reaction barrier (in eV) to form OCOO from adsorbed O₂ and CO is

$$E^{R3} = 0.52 \cdot \Delta E_1 + 0.34 \quad (12)$$

where ΔE_1 is

$$\Delta E_1 = E_{\text{OCO}} - E_{\text{CO}} - E_{\text{O}_2} \quad (13)$$

where

$$E_{\text{OCO}} = 1.10 \cdot E_{\text{CO}} - 0.36 \quad (14)$$

The reaction barrier (in eV) for the decomposition of OCOO is given by

$$E^{R4} = -0.53 \cdot \Delta E_2 - 1.00 \quad (15)$$

where ΔE_2 is

$$\Delta E_2 = 0.64 \cdot \Delta E_1 - 2.54 \quad (16)$$

The reaction barrier (in eV) for the reaction of CO with atomic O is

$$E^{R5} = 0.76 \cdot \Delta E_1 + 0.51 \quad (17)$$

Besides the adsorption, desorption, and reaction events, adsorbates diffuse over the surface. The diffusion barriers are low over Au and diffusion barriers for CO and O have been increased to 0.4 eV to reduce the number of diffusion events. However, the rate for the diffusion events is still several orders of magnitude higher than the reaction rates, which indicates that the increased barriers do not affect the reaction kinetics. The diffusion for CO from a Pt site to an Au site is set to the difference in adsorption energy over these sites, which is 1.4 eV. We do not include adsorbate–adsorbate interactions, which is motivated by the low coverages over both the Au and Pt@Au systems (see the Supporting Information).

RESULTS AND DISCUSSION

Low-temperature CO oxidation over Au is experimentally well established⁸ and has previously been studied computationally using mean-field models.^{11,20,21} Here, we compute the temperature dependence on the TOF for pure Au systems (Figure 2) as a reference for dilute Pt@Au alloys. The TOF is

calculated as the number of formed CO₂ molecules per second and the number of surface atoms.

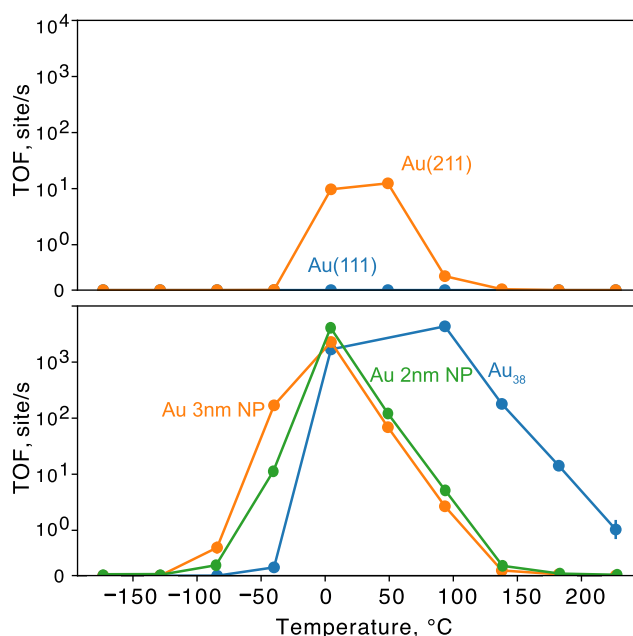


Figure 2. Temperature-dependent TOF for Au(111) and Au(211) [top] and for Au₃₈ together with the two Au NPs [bottom]. The simulations are obtained with a total pressure of 40 Torr under lean conditions ($p_{\text{O}_2}/p_{\text{CO}}$ is 5).

The TOF for Au(111) is close to zero over the entire temperature range. The low activity is a result of the weak adsorption energies for both CO and O₂ on Au(111). Thus, the CO and O₂ coverages are close to zero in the temperature range where the rates of the oxidation steps are appreciable. An activity for CO oxidation is instead calculated for Au(211), which has under-coordinated sites and, consequently, higher adsorption energies. The rate is nonzero between −50 and 100 °C. This result is consistent with previous mean-field treatments of the reaction.^{11,20}

The Au₃₈ cluster and the Au NPs show activity in a wider temperature range than does Au(211). The Au₃₈ cluster is active over 300° with high activity already at −50 °C. The Au NPs have activities at even lower temperatures and are active until 100 °C. The higher onset temperature for Au₃₈ compared to that for the Au NPs is related to the stability of adsorbed OCOO, which start to decompose on Au₃₈ at −75 °C. The wider temperature range for the activity on Au₃₈ is traced to the stronger bonding of the adsorbates and, consequently, the possibility to have coverages of CO and O₂ at higher temperatures.

The bare gold systems with under-coordinated sites show activity at temperatures as low as −100 °C. It is clear that the activity is strongly structure-dependent and, therefore, difficult to compare with experiments where the structure is unknown. Moreover, the effect of the support in experiments may influence the reaction via modification of the Au structure as well as charge transfers and reactions at the Au/support interface. We note that Au-catalysts have been measured to have activity at temperatures as low as −80 °C.^{8,9} Our results show activity at temperatures as low as −100 °C, which could be related to an uncertainty in the adsorption and reaction

energies caused by the applied exchange–correlation functional.²⁸

To elucidate the fundamental difference of CO oxidation over Au(111) and a system with under-coordinated sites, we analyze the rates of the elementary reactions (Figure 3). For

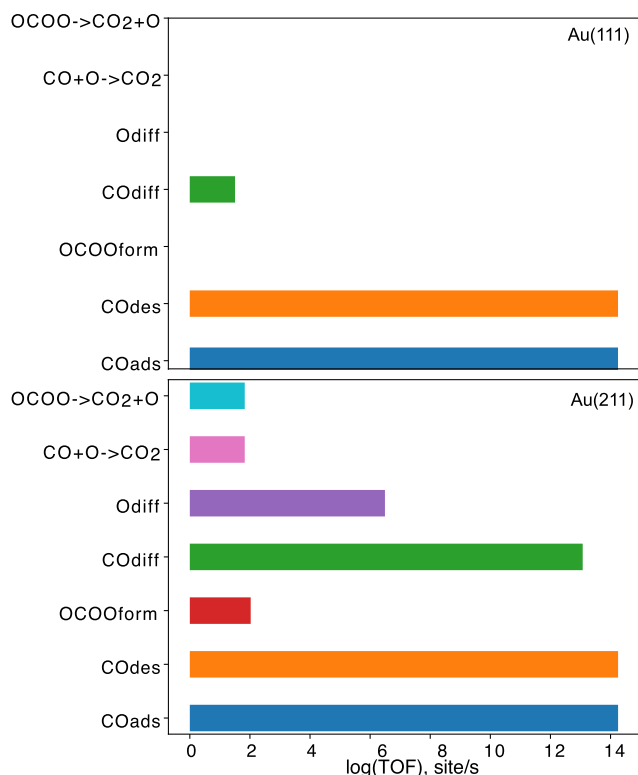


Figure 3. TOF for the elementary reaction. The simulations are obtained at 27 °C (300 K) with a total pressure of 40 Torr under lean conditions ($p_{\text{O}_2}/p_{\text{CO}}$ is 5).

Au(111), the main events are CO adsorption and desorption. CO may diffuse before it desorbs. The equilibrium coverage for O₂ is in this case about 10^{−9}. CO adsorption and desorption are the main events also for Au(211); however, the O₂ equilibrium coverage is in this case about 10^{−5}, which enables OCOO formation. OCOO decomposition yields CO₂ and adsorbed O. Atomic O reacts with CO to form a second form of CO₂. The lower adsorption energy of CO on Au(211) compared to that on Au(111) results in more CO diffusion events. Adsorbed atomic O may also diffuse before it reacts to form CO₂.

Having established the properties for bare Au systems, we investigated the effect of having Pt embedded in the Au hosts. The TOFs for Pt@Au(111), Pt@Au(211), and Pt placed in two different positions in the Au NPs are shown in Figure 4. The presence of a Pt monomer has no effect on the close-packed Au(111) system, which remains inactive over the entire temperature range. The Pt@Au(211) system is active from −100 °C and has an activity that extends to 200 °C. The TOF over Pt@Au(211) originates from the fact that CO adsorbs on the Pt site, which enables OCOO formation as long as the coverage of O₂ is high enough. Pt@Au(211) is fundamentally different from Au(211) because of the low adsorption energy of CO on the Pt site. The coverage of CO is close to one on the Pt site over the entire temperature interval (see Supporting Information).

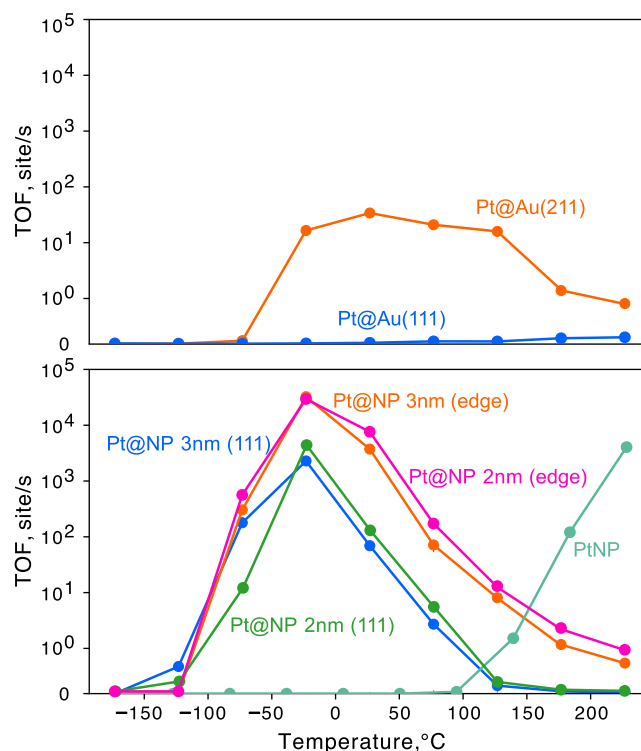


Figure 4. Temperature-dependent TOF for Pt@Au(111) and Pt@Au(211) [top] and Pt@NP(111) and Pt@NP(edge) [bottom]. The results for the NPs are compared with the results of a pure Pt NP. The simulations are obtained with a total pressure of 40 Torr under lean conditions ($p_{\text{O}_2}/p_{\text{CO}}$ is 5).

The temperature range for activity of Pt@NP(111) is similar to that of the pure Au NPs systems. Because of the low O₂ adsorption energy on (111) facets, the presence of CO on the Pt monomer does not appreciably affect the TOF. The situation is different when Pt is placed on the edges of the NPs. With Pt in an edge position, the TOF is higher by 1 order of magnitude than for the corresponding pure Au-systems. Moreover, the temperature window of the activity is wider. The differences are clearly related to the higher coverage of CO. As for the extended surfaces, the CO coverage on the Pt site is close to one in the entire temperature range (see Supporting Information) and the activity in the high temperature range is determined by the availability of adsorbed O₂.

The results for the NP systems are compared to the case with a Pt-only particle of the same shape and size as the 3.2 nm Au NP (parameters and scaling relations in Supporting Information). The Pt particle has an appreciable TOF only at temperatures above 100 °C, which is a consequence of the self-poisoning of CO, which prevents the dissociated adsorption of O₂. Moreover, the reaction barriers for CO₂ formation are higher over the Pt-only system compared to those in the dilute alloys.

The rates of the elementary reactions over Pt@Au(111) and Pt@Au(211) are shown in Figure 5. Here, the events on the Pt and Au sites are combined. The main difference between Au(111) (Figure 3) and Pt@Au(111) is the possibility to have a CO coverage, which enables OCOO formation. Once OCOO decomposes, atomic O is formed, which may diffuse over the surface. The rates for Pt@Au(211) are similar to those for Au(211). There is a difference in the amount of

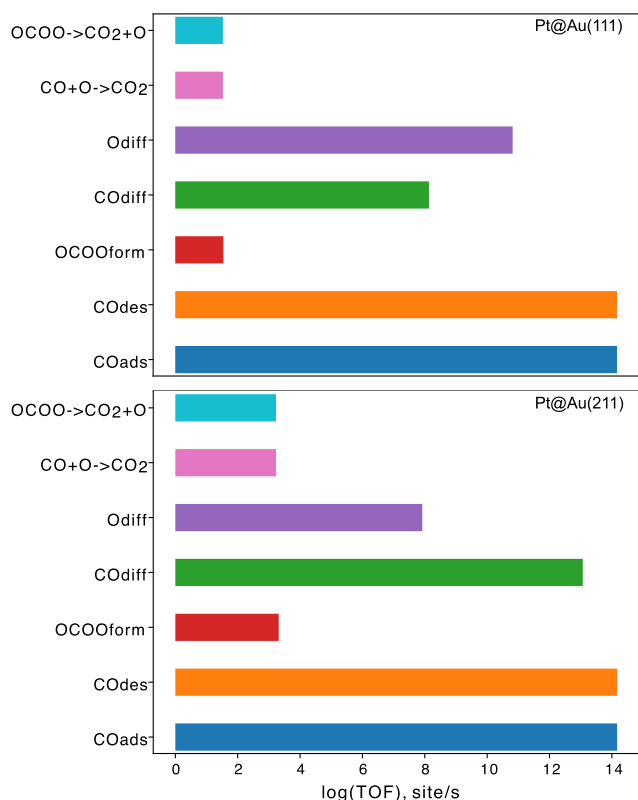


Figure 5. TOF for the elementary reaction over Pt@Au(111) and Pt@Au(211). The simulations are obtained at 27 °C (300 K) with a total pressure of 40 Torr under lean conditions ($p_{\text{O}_2}/p_{\text{CO}}$ is 5).

formed OCOO, which affects the rates of OCOO decomposition and CO oxidation with adsorbed O.

CONCLUSIONS

We have used first-principles-based kMC simulations to explore CO oxidation over pure Au systems and dilute alloys of Pt embedded in extended Au hosts and Au NP. Low-coordinated Au sites show activity at temperatures below 0 °C, which is in agreement with the experimental evidence of low-temperature activity of Au NPs. The activity decays above 100 °C because of the low coverage of both CO and O₂. Embedding Pt in the Au hosts widens the range of activity as the reaction is not limited by a low coverage of CO. Combining dilute Pt@Au alloys and pure Pt NP would enable CO oxidation at both low and high temperatures.

ASSOCIATED CONTENT

Supporting Information

The Supporting Information is available free of charge at <https://pubs.acs.org/doi/10.1021/acs.jpcc.4c01263>.

Scaling relations for CO adsorption on Au systems, CO coverage on selected Pt@Au systems and parameters, and scaling relations for the Pt NP simulations (PDF) Atomic structures for the considered systems (ZIP)

AUTHOR INFORMATION

Corresponding Author

Henrik Grönbeck – Department of Physics and Competence Centre for Catalysis, Chalmers University of Technology,

Göteborg SE-412 96, Sweden; orcid.org/0000-0002-8709-2889; Email: ghj@chalmers.se

Author

Noemi Bosio – Department of Physics and Competence Centre for Catalysis, Chalmers University of Technology, Göteborg SE-412 96, Sweden

Complete contact information is available at: <https://pubs.acs.org/10.1021/acs.jpcc.4c01263>

Notes

The authors declare no competing financial interest.

ACKNOWLEDGMENTS

The calculations have been performed at NSC (Linköping) and PDC (Stockholm) through a NAISS grant (NAISS 2023/3-29). Financial support from the Swedish Research Council (2020-05191) is acknowledged. The Competence Centre for Catalysis (KCK) is hosted by Chalmers University of Technology and financially supported by the Swedish Energy Agency (52689-1) and the member companies Johnson Matthey, Perstorp, Powercell, Preem, Scania CV, Umicore, and Volvo Group.

REFERENCES

- (1) Shelef, M.; McCabe, R. W. Twenty-five years after introduction of automotive catalysts: what next? *Catal. Today* **2000**, *62*, 35–50.
- (2) Lenaers, G. On-board real life emission measurements on a 3 way catalyst gasoline car in motor way-rural-and city traffic and on two Euro-1 diesel city buses. *Sci. Total Environ.* **1996**, *189–190*, 139–147.
- (3) van Spronsen, M. A.; Frenken, J. W. M.; Groot, I. M. N. Surface science under reaction conditions: CO oxidation on Pt and Pd model catalysts. *Chem. Soc. Rev.* **2017**, *46*, 4347–4374.
- (4) Skoglundh, M.; Fridell, E. Strategies for Enhancing Low-Temperature Activity. *Top. Catal.* **2004**, *28*, 79–87.
- (5) Bosio, N.; Di, M.; Skoglundh, M.; Carlsson, P.-A.; Grönbeck, H. Interface Reactions Dominate Low-Temperature CO Oxidation Activity over Pt/CeO₂. *J. Phys. Chem. C* **2022**, *126*, 16164–16171.
- (6) An, K.; Alayoglu, S.; Musselwhite, N.; Plamthottam, S.; Melaet, G.; Lindeman, A. E.; Somorjai, G. A. Enhanced CO oxidation rates at the interface of mesoporous oxides and Pt nanoparticles. *J. Am. Chem. Soc.* **2013**, *135*, 16689–16696.
- (7) Doornkamp, C.; Ponc, V. The universal character of the Mars and Van Krevelen mechanism. *J. Mol. Catal. A: Chem.* **2000**, *162*, 19–32.
- (8) Haruta, M.; Yamada, N.; Kobayashi, T.; Iijima, S. Gold catalysts prepared by coprecipitation for low-temperature oxidation of hydrogen and of carbon monoxide. *J. Catal.* **1989**, *115*, 301–309.
- (9) Ramirez Reina, T.; Ivanova, S.; Centeno, M. A.; Odriozola, J. Low-temperature CO oxidation on multicomponent gold based catalysts. *Front. Chem.* **2013**, *1*, 12.
- (10) Janssens, T. V. W.; Clausen, B. S.; Hvolbæk, B.; Falsig, H.; Christensen, C. H.; Bligaard, T.; Nørskov, J. K. Insights into the reactivity of supported Au nanoparticles: combining theory and experiments. *Top. Catal.* **2007**, *44*, 15–26.
- (11) Falsig, H.; Hvolbæk, B.; Kristensen, I. S.; Jiang, T.; Bligaard, T.; Christensen, C. H.; Nørskov, J. K. Trends in the catalytic CO oxidation activity of nanoparticles. *Angew. Chem., Int. Ed.* **2008**, *47*, 4835–4839.
- (12) Sandoval, A.; Aguilar, A.; Louis, C.; Traverse, A.; Zanella, R. Bimetallic Au–Ag/TiO₂ catalyst prepared by deposition–precipitation: high activity and stability in CO oxidation. *J. Catal.* **2011**, *281*, 40–49.
- (13) Song, Y.-J.; Lopez-De Jesus, Y. M.; Fanson, P. T.; Williams, C. T. Preparation and characterization of dendrimer-derived bimetallic

Ir–Au/Al₂O₃ catalysts for CO oxidation. *J. Phys. Chem. C* **2013**, *117*, 10999–11007.

(14) Peng, Z.; Yang, H. PtAu bimetallic heteronanostructures made by post-synthesis modification of Pt-on-Au nanoparticles. *Nano Res.* **2009**, *2*, 406–415.

(15) Xu, Y.; Liu, L.; Chong, H.; Yang, S.; Xiang, J.; Meng, X.; Zhu, M. The key gold: enhanced platinum catalysis for the selective hydrogenation of α , β -unsaturated ketone. *J. Phys. Chem. C* **2016**, *120*, 12446–12451.

(16) Lucci, F. R.; Darby, M. T.; Mattera, M. F. G.; Ivimey, C. J.; Therrien, A. J.; Michaelides, A.; Stamatakis, M.; Sykes, E. C. H. Controlling hydrogen activation, spillover, and desorption with Pd–Au single-atom alloys. *J. Phys. Chem. Lett.* **2016**, *7*, 480–485.

(17) Lang, L.; Pan, Z.; Yan, J. Ni–Au alloy nanoparticles as a high performance heterogeneous catalyst for hydrogenation of aromatic nitro compounds. *J. Alloys Compd.* **2019**, *792*, 286–290.

(18) Jørgensen, M.; Grönbeck, H. Selective acetylene hydrogenation over single-atom alloy nanoparticles by kinetic Monte Carlo. *J. Am. Chem. Soc.* **2019**, *141*, 8541–8549.

(19) Svensson, R.; Grönbeck, H. Site-Communication in Direct Formation of H₂O₂ over Single Atom Pd@Au Nanoparticles. *J. Am. Chem. Soc.* **2023**, *145*, 11579–11588.

(20) Jiang, T.; Mowbray, D. J.; Dobrin, S.; Falsig, H.; Hvolbaek, B.; Bligaard, T.; Nørskov, J. K. Trends in CO Oxidation Rates for Metal Nanoparticles and Close-Packed, Stepped, and Kinked Surfaces. *J. Phys. Chem. C* **2009**, *113*, 10548–10553.

(21) Liu, J.-X.; Filot, I. A. W.; Su, Y.; Zijlstra, B.; Hensen, E. J. M. Optimum particle size for gold-catalyzed CO oxidation. *J. Phys. Chem. C* **2018**, *122*, 8327–8340.

(22) Nikbin, N.; Austin, N.; Vlachos, D. G.; Stamatakis, M.; Mpourmpakis, G. Catalysis at the sub-nanoscale: complex CO oxidation chemistry on a few Au atoms. *Catal. Sci. Technol.* **2015**, *5*, 134–141.

(23) Kresse, G.; Hafner, J. Ab initio molecular dynamics for liquid metals. *Phys. Rev. B* **1993**, *47*, 558–561.

(24) Kresse, G.; Furthmüller, J. Efficiency of ab-initio total energy calculations for metals and semiconductors using a plane-wave basis set. *Comput. Mater. Sci.* **1996**, *6*, 15–50.

(25) Kresse, G.; Furthmüller, J. Efficient iterative schemes for ab initio total-energy calculations using a plane-wave basis set. *Phys. Rev. B* **1996**, *54*, 11169–11186.

(26) Blöchl, P. E. Projector augmented-wave method. *Phys. Rev. B* **1994**, *50*, 17953–17979.

(27) Kresse, G.; Joubert, D. From ultrasoft pseudopotentials to the projector augmented-wave method. *Phys. Rev. B* **1999**, *59*, 1758–1775.

(28) Perdew, J. P.; Burke, K.; Ernzerhof, M. Generalized gradient approximation made simple. *Phys. Rev. Lett.* **1996**, *77*, 3865–3868.

(29) Grimme, S.; Antony, J.; Ehrlich, S.; Krieg, H. A consistent and accurate ab initio parametrization of density functional dispersion correction (DFT-D) for the 94 elements H–Pu. *J. Chem. Phys.* **2010**, *132*, 154104.

(30) Monkhorst, H. J.; Pack, J. D. Special points for Brillouin-zone integrations. *Phys. Rev. B* **1976**, *13*, 5188–5192.

(31) Pack, J. D.; Monkhorst, H. J. Special points for Brillouin-zone integrations—a reply. *Phys. Rev. B* **1977**, *16*, 1748–1749.

(32) Jansen, A. P. J. *An introduction to Monte Carlo simulations of surface reactions*; Springer-Verlag: Berlin, Heidelberg, 2003.

(33) Jørgensen, M.; Grönbeck, H. MonteCoffee: A programmable kinetic Monte Carlo framework. *J. Chem. Phys.* **2018**, *149*, 114101.

(34) Tsuda, Y.; Gueriba, J. S.; Ueta, H.; Diño, W. A.; Kurahashi, M.; Okada, M. Probing Copper and Copper–Gold Alloy Surfaces with Space-Quantized Oxygen Molecular Beam. *J. Am. Chem. Soc. Au* **2022**, *2*, 1839–1847.

(35) Bosio, N.; Grönbeck, H. Sensitivity of Monte Carlo Simulations to Linear Scaling Relations. *J. Phys. Chem. C* **2020**, *124*, 11952–11959.

(36) Jørgensen, M.; Grönbeck, H. Adsorbate entropies with complete potential energy sampling in microkinetic modeling. *J. Phys. Chem. C* **2017**, *121*, 7199–7207.

(37) Eyring, H. The activated complex and the absolute rate of chemical reactions. *Chem. Rev.* **1935**, *17*, 65–77.

(38) Abild-Pedersen, F.; Andersson, M. P. CO adsorption energies on metals with correction for high coordination adsorption sites—A density functional study. *Surf. Sci.* **2007**, *601*, 1747–1753.

(39) Hammer, B.; Nørskov, J. Theoretical surface science and catalysis - Calculations and concepts. *Adv. Catal.* **2000**, *45*, 71–129.

(40) Nørskov, J.; Bligaard, T.; Logadottir, A.; Bahn, S.; Hansen, L.; Bollinger, M.; Bengaard, H.; Hammer, B.; Sljivancanin, Z.; Mavrikakis, M.; Xu, Y.; Dahl, S.; Jacobsen, C. Universality in heterogeneous catalysis. *J. Catal.* **2002**, *209*, 275–278.

(41) Calle-Vallejo, F.; Martínez, J. I.; García-Lastra, J. M.; Sautet, P.; Loffreda, D. Fast prediction of adsorption properties for platinum nanocatalysts with generalized coordination numbers. *Angew. Chem., Int. Ed.* **2014**, *53*, 8316–8319.